CARD9 in neutrophils protects from colitis and controls mitochondrial metabolism and cell survival

Camille Danne, Chloé Michaudel, Jurate Skerniskyte, Julien Planchais,
Aurélie Magniez, Allison Agus, Marie-Laure Michel, Bruno Lamas, Gregory
da Costa, Madeleine Spatz, et al.

▶ To cite this version:

HAL Id: hal-03791244
https://hal.inrae.fr/hal-03791244v2

CARD9 in Neutrophils Protects from Colitis and Controls Mitochondrial Metabolism and Cell Survival

Camille Danne, Chloé Michaudel, Jurate Skerniskyte, Julien Planchais, Aurélie Magniez, Allison Agus, Marie Laure Michel, Bruno Lamas, Gregory Da Costa, Madeleine Spatz, et al.

To cite this version:

HAL Id: hal-03774214

https://ut3-toulouseinp.hal.science/hal-03774214

Preprint submitted on 9 Sep 2022

1   **CARD9 in Neutrophils Protects from Colitis**

2   **and Controls Mitochondrial Metabolism and Cell Survival**

3

4   Camille Danne[1,2,3*], Chloé Michaudel[1,3], Jurate Skerniskyte[4], Julien Planchais[1,3], Aurélie Magniez[1,3],

5   Allison Agus[1,3], Marie-Laure Michel[1,3], Bruno Lamas[1,3], Gregory Da-Costa[1,3], Madeleine Spatz[1,3],

6   Cyriane Oeuvray[2,3], Chloé Galbert[2,3], Maxime Poirier[1,3], Yazhou Wang[1,3], Alexia Lapiere[1,3], Nathalie

7   Rolhion[2,3], Tatiana Ledent[2], Cédric Pionneau[5], Solenne Chardonnet[5], Floriant Bellvert[6], Edern

8   Cahoreau[6], Amandine Rocher[6], Rafael Jose Argüello[7], Carole Peyssonnaux[8], Sabine Louis[8], Mathias

9   L.-Richard[1,3], Philippe Langella[1,3], Jamel El-Benna[9], Benoit Marteyn[4,10,11], Harry Sokol[1,2,3*]

10

11   [1] Université Paris-Saclay, INRAE, AgroParisTech, Micalis Institute, Jouy-en-Josas, France

12   [2] Sorbonne Université, INSERM UMRS-938, Centre de Recherche Saint-Antoine, CRSA, AP-HP,

13   Hôpital Saint-Antoine, Service de Gastroentérologie, F-75012 Paris, France

14   [3] Paris Center for Microbiome Medicine (PaCeMM) FHU, Paris, France

15   [4] CNRS, UPR 9002, Université de Strasbourg, Institut de Biologie Moléculaire et Cellulaire,

16   Architecture et Réactivité de l'ARN, Strasbourg, France

17   [5] Sorbonne Université, Inserm, UMS PASS, Plateforme Post-génomique de la Pitié Salpêtrière (P3S),

18   Paris, France

19   [6] MetaToul-MetaboHUB, National Infrastructure of Metabolomics & Fluxomics (ANR-11-INBS-0010),

20   31077 Toulouse, France

21   [7] Aix Marseille Univ, CNRS, INSERM, CIML, Centre d'Immunologie de Marseille-Luminy, Marseille,

22   France

23   [8] Institut Cochin, Inserm, CNRS, Université de Paris, Laboratoire d'excellence GR-Ex, Paris, France

24   [9] Université de Paris, INSERM-U1149, CNRS-ERL8252, Centre de Recherche sur l'Inflammation

25   (CRI), Laboratoire d'Excellence Inflamex, Faculté de Médecine Xavier Bichat, Paris, France

26   [10] University of Strasbourg Institute for Advanced Study (USIAS), Strasbourg, France

27   [11] Institut Pasteur, Université de Paris, Inserm 1225 Unité de Pathogenèse des Infections Vasculaires,

28   28 rue du Dr. Roux, 75724 Paris Cedex 15, France

29

30   *Co-Corresponding Authors: Camille Danne, PhD, Centre de Recherche Saint-Antoine, 27 rue

31   Chaligny, 75012 Paris, France (camille.danne@gmail.com) and Harry Sokol, MD, PhD, Service de

32   Gastro-entérologie, Hôpital Saint-Antoine, 184 rue du Faubourg Saint-Antoine, 75571 Paris Cedex 12,

33   France (harry.sokol@aphp.fr).

34

35

38

39

ABSTRACT

41   **Objectives** : Inflammatory bowel disease (IBD) results from a combination of genetic predisposition,

42   dysbiosis of the gut microbiota and environmental factors, leading to alterations in the gastrointestinal

43   immune response and chronic inflammation. Caspase recruitment domain 9 (*Card9*), one of the IBD

44   susceptibility genes, has been shown to protect against intestinal inflammation and fungal infection.

45   However, the cell types and mechanisms involved in the CARD9 protective role against inflammation

46   remain unknown.

47   **Design** : We used dextran sulfate sodium (DSS)-induced and adoptive transfer colitis models in total

48   and conditional CARD9 knock-out mice to uncover which cell types play a role in the CARD9

49   protective phenotype. The impact of *Card9* deletion on neutrophil function was assessed by an *in vivo*

50   model of fungal infection and various functional assays, including endpoint dilution assay, apoptosis

51   assay by flow cytometry, proteomics and real time bioenergetic profile analysis (Seahorse).

52   **Results** : Lymphocytes are not intrinsically involved in the CARD9 protective role against colitis.

53   CARD9 expression in neutrophils, but not in epithelial or CD11c+ cells, protects against DSS-induced

2

54   colitis. In the absence of CARD9, mitochondrial dysfunction in neutrophils leads to their premature

55   death through apoptosis, especially in oxidative environment. The decrease of fonctional neutrophils in

56   tissues could explain the impaired containment of fungi and increased susceptibility to intestinal

57   inflammation.

58   **Conclusion** : These results provide new insight into the role of CARD9 in neutrophil mitochondrial

59   function and its involvement in intestinal inflammation, paving the way for new therapeutic strategies

60   targeting neutrophils.

61

62

63   **Summary box**

64   1. **What is already known about this subject?**

65   •   Inflammatory bowel disease (IBD) results from genetic predisposition, microbiota dysbiosis

66   and environmental factors, but the alterations of the immune response leading to chronic

67   intestinal inflammation are still not fully understood.

68   •   Caspase recruitment domain 9 (*Card9*), one of the IBD susceptibility genes, has been shown

69   to protect against intestinal inflammation and fungal infection.

70   •   However, the cell types and cellular mechanisms involved in the CARD9 protective role

71   against inflammation remain unknown.

72   2. **What are the new findings?**

73   •   CARD9 expression in neutrophils, but not in lymphocytes, epithelial cells or CD11c+ cells,

74   protects against DSS-induced colitis.

75   •   In the absence of CARD9, mitochondrial dysfunction in neutrophils leads to their premature

76   death through apoptosis, especially in oxidative environment.

77   •   The decrease of fonctional neutrophils in tissues could explain the impaired containment of

78   fungi and increased susceptibility to intestinal inflammation.

79   3. **How might it impact on clinical practice in the foreseeable future?**

80   •   These results provide new insight into the role of CARD9 in neutrophil mitochondrial function

81   and its involvement in intestinal inflammation.

82   •   Understanding the role of neutrophils in chronic inflammation could lead to innovative

83   therapeutic strategies targeting these key immune cells for various complex diseases.

84

85 **INTRODUCTION**

86   Inflammatory bowel disease (IBD) results from a combination of genetic predisposition,

87 dysbiosis of the gut microbiota and environmental factors, leading to alterations in the gastrointestinal

88 immune response and chronic inflammation[1,2]. Especially, the innate compartment of the immune

89 system has been involved in IBD development, with a role for dendritic cells, macrophages and

90 neutrophils[3–6]. Neutrophils, one of the most abundant and important mediators of innate immunity, are

91 professional phagocytes that mount the acute inflammatory response and act as the first line of

92 defense against invading pathogens[7,8]. An impaired neutrophil function may result in limited pathogen

93 clearance and fuel a chronic inflammatory response with excessive lymphocyte activation. Patients

94 with congenital disorders in neutrophil function such as chronic granulomatous disease (CGD) often

95 develop IBD-like phenotypes[9–12]. Moreover, functional defects have been observed in neutrophils from

96 IBD patients, including impaired chemotaxis, migration, phagocytosis or ROS production[4,5].

97   CARD9, one of the numerous IBD susceptibility genes, encodes an adaptor protein that

98 integrates signals downstream of pattern recognition receptors [13–18]. Especially, CARD9 is involved in

99 the host defense against fungi via C-type lectin sensing[19,20]. CARD9 polymorphisms in humans are

100 associated with multiple susceptibilities including IBD[21], whereas loss-of-function mutations are

101 associated with invasive fungal infections caused by species such as *Candida albicans*[21–24]. CARD9

102 was shown to mediate its protective functions, at least in part, through the induction of adaptive Th17

103 cell responses[22,23,25]. *Card9*^{−/−} mice are more susceptible to colitis due to impaired IL-22 production

104 and have an increased load of gut-resident fungi[25]. Indeed, CARD9 affects the composition and

105 function of the gut microbiota, altering the production of anti-inflammatory microbial metabolites[26,27].

106 However, the cell types involved in the CARD9 protective role against intestinal inflammation remain

107 unknown.

108   In this work, we show that CARD9 expression in neutrophils, but not in epithelial or CD11c+

109 cells such as dendritic cells, protects against dextran sulfate sodium (DSS)-induced colitis in mice.

110 The absence of CARD9 impacts neutrophil capacity to contain fungal dissemination, notably by

111 impairing neutrophil mitochondrial function and survival. Indeed, *Card9* deletion induces a basal

112 overactivation of mitochondria, increasing mitochondrial dysfunction and apoptosis in neutrophils.

113   These results provide new insight into the role of CARD9 in neutrophil mitochondrial function and its

114   consequences in intestinal inflammation.

115

116   **RESULTS**

117   **Lymphocytes have no intrinsic role in the *Card9*$^{-/-}$ susceptibility to colitis**

118   CARD9 was previously reported to be mainly expressed in myeloid cells, especially dendritic

119   cells, macrophages and neutrophils[14,28]. Using qRT-PCR analyses in various C57BL/6 mouse organs,

120   we confirmed that *Card9* is mainly expressed in immune organs such as bone marrow, spleen and

121   distal small intestine (ileum), but is low at baseline in proximal and mid small intestine, caecum, colon,

122   stomach and liver, and not detectable in *Card9*$^{-/-}$ tissues (Fig. S1A). Consistently, western-blot analysis

123   showed the expression of CARD9 protein in bone marrow, spleen and distal small intestine of WT

124   mice (Fig. S1B). To dissect *Card9* expression at the cellular level, we sorted immune cell populations

125   from spleen and bone marrow of WT mice. *Card9* is highly expressed in neutrophils (Ly6G^{+}CD11b^{+}

126   cells), macrophages (CD11b^{+}F4/80^{+} cells), CD11c^{+} cells, including dendritic cells, and monocytes

127   (CD11b^{hi}F4/80^{+} cells) ; but the expression is lower in innate or adaptive lymphocytes (CD3^{+}TCRγδ^{+}

128   lymphoid cells, CD3^{+}CD4^{+} and CD3^{+}CD8^{+} T cells, CD3^{-}CD19^{+} B cells) (Fig. S1C). Thus, CARD9 likely

129   plays a major role within the myeloid immune compartment.

130   Previous studies from our group and others started to investigate the role of *Card9* in murine

131   models of experimental colitis, showing that *Card9* deletion increases colitis susceptibility[25,26,29]. In

132   order to decipher the respective roles of lymphocytes and myeloid cells in the *Card9* susceptibility to

133   intestinal injury and inflammation, we first induced colitis with DSS in *Rag2*$^{-/-}$ and *Rag2*$^{-/-}$x*Card9*$^{-/-}$ mice

134   that are deficient in functional T and B cells. Mice were euthanized after receiving 3% DSS in drinking

135   water for 7d, as the severity limit was reached for the *Rag2*$^{-/-}$x*Card9*$^{-/-}$ group. Indeed, desease severity

136   (defined by weight loss, DAI (Disease Activity Index) score, colon length, and histologic score) was

137   strongly increased in *Rag2*$^{-/-}$x*Card9*$^{-/-}$ mice compared to *Rag2*$^{-/-}$ mice (Fig. 1A-E). In an adoptive

138   transfer model of colitis, in which *Rag2*$^{-/-}$ mice lacking functional lymphocytes received T cells either

139   from WT or *Card9*$^{-/-}$ mice, no difference was observed on colitis severity (Fig. 1F), meaning that *Card9*

140   expression in T cells does not impact colitis susceptibility. However, the transfer of WT T cells into

141   *Rag2*$^{-/-}$x*Card9*$^{-/-}$ recipient mice did aggravate colitis compared to *Rag2*$^{-/-}$ simple KO recipients, with a

5

142   significantly stronger weight loss (Fig. 1F). These results demonstrate that *Card9* mediates its

143   protective role against colitis through the innate immunity compartment, although its role in intestinal

144   epithelial cells cannot be ruled out.

145

146   **_Card9_ expression in neutrophils, but not in epithelial or CD11c$^+$ cells, protects against colitis**

147   Based on these findings, we generated conditional KO mice using the cre-lox technology, and

148   obtained mouse strains defective for *Card9* either in epithelial cells only (Villincrex*Card9*lox line),

149   CD11c-expressing cells only, including dendritic cells, macrophages and monocytes

150   (CD11ccrex*Card9*lox line), or neutrophils only (Mrp8crex*Card9*lox line). To validate their phenotypes,

151   we isolated epithelial cells from the colonic lamina propria of *Card9*^{Villincre} and *Card9*^{Villinwt} mice, or used

152   MACS separation columns to isolate either CD11c$^+$ or Ly6G$^+$ cell fractions from spleen or bone marrow

153   of *Card9*^{CD11cwt} and *Card9*^{CD11ccre} mice or *Card9*^{Mrp8wt} and *Card9*^{Mrp8cre} mice, respectively. We

154   performed qRT-PCR on these cell fractions (Fig. S2A), and western-blot analyses on the Ly6G$^+$ and

155   Ly6G$^{low/-}$ fractions of *Card9*WT, *Card9*$^{-/-}$, *Card9*^{Mrp8wt} and *Card9*^{Mrp8cre} mice (Fig. S2B). Results

156   confirmed that *Card9* deletion is restricted to the expected cell types (Fig. S2A-B). Purity of

157   Ly6G$^+$CD11b$^+$ neutrophils isolated from the bone marrow of C57Bl/6 mice reached 95% by flow

158   cytometry (Fig. S2C).

159   We then assessed the susceptibility of these newly generated mice strains in a model of

160   intestinal inflammation. DSS was administered for 7 days, followed by additional 5 days in which DSS

161   was discontinued. The deletion of *Card9* in epithelial or CD11c$^+$ cells did not affect mouse

162   susceptibility to colitis (Fig. 2A-B and S2D). However, the deletion of *Card9* in neutrophils aggravates

163   colitis compared to WT littermate controls, with significantly increased weight loss from day 8 (Fig.

164   2C), DAI score from day 5 (Fig. 2C), and histological score (Fig. 2E-F), as well as decreased colon

165   length (Fig. 2D). Thus, the expression of *Card9* in neutrophils plays a crucial role in the protection

166   against intestinal inflammation. The expression of myeloperoxidase (MPO), an anti-microbial enzyme

167   abundantly expressed in neutrophils, was increased in *Card9*^{Mrp8cre} compared to *Card9*^{Mrp8wt} colon

168   tissue at day 12, indicating a more important presence or activation of neutrophils in the absence of

169   *Card9* (Fig. 2G). Similarly, the expression of the inflammatory marker lipocalin (*Lcn2*) was increased in

170   *Card9*^{Mrp8cre} colon tissue at day 12 (Fig. 2H).

171   These results suggest that *Card9*-deficient neutrophils are efficiently recruited to the inflamed

172   tissue but likely exhibit functional defects preventing them from adequately controlling microbial

173   invaders and thus maintaining inflammation within the intestinal mucosa. We previously showed that

174   the gut microbiota of total *Card9*^{-/-} KO lineage mice exhibit an altered production of AhR agonists

175   compared to WT[26]. However, no difference was observed between *Card9*[Mrp8wt] and *Card9*[Mrp8cre] mice

176   (Fig. S2E), suggesting that this aspect of the phenotype is not intrinsically related to the role of CARD9

177   in neutrophils.

178

179   **Card9 deletion affects the number of activated neutrophils in the inflamed colon**

180   To investigate neutrophil function in WT mice during DSS-induced inflammation, we analyzed

181   RNA expression of the neutrophil-specific genes *Lcn2*, *Cxcr2* and *S100A8* in colon tissue at days 0, 4,

182   7, 9, 12 and 16 of DSS-induced colitis (Fig. 3A and S2F). The neutrophil recruitment was maximal at

183   day 9, corresponding to the peak of clinical inflammation, and remained high up to day 16 (Fig. 3A).

184   Histological sections of the distal colon confirmed these findings (Fig. 3B). The fact that inflammation

185   was higher in *Card9*[Mrp8cre] than in *Card9*[Mrp8wt] mice (Fig. S2E), and that *Lcn2*, *Cxcr2* and *S100a8*

186   expression at day 9 in colon tissue were similar in both genotypes (Fig. 3C) excludes the hypothesis of

187   a defect of neutrophil recruitment in *Card9*[Mrp8cre] mice. We then examined the immune cell populations

188   recruited to the colon lamina propria (LP) of *Card9*[Mrp8cre] versus *Card9*[Mrp8wt] mice at day 9 of colitis.

189   Surprisingly, although the total number of neutrophils was similar in the two genotypes, the percentage

190   and count of mature and activated Ly6G^{+}CD11b^{+} neutrophils was decreased in the colon LP of

191   *Card9*[Mrp8cre] (Fig. 3D-E). Moreover, the expression levels of both Ly6G and CD11b surface proteins,

192   two major neutrophil maturationa and activation markers, were significantly reduced in the overall

193   neutrophil population, as shown by decreased MFIs (for Mean Fluorescence Intensity) (Fig. 3F-G).

194   These findings suggest a structural or functional defect in neutrophils deleted for *Card9*.

195

196   **C. albicans killing capacities are impacted by Card9 deletion in neutrophils**

197   To investigate the defect caused by *Card9* deletion in *Card9*[Mrp8cre] compared to *Card9*[Mrp8wt]

198   neutrophils, we developed several *in vitro* assays with Ly6G^{+} neutrophils purified from mouse bone

199   marrow using MACS separation columns. Immunofluorescence, scanning electron microscopy (SEM)

200   and transmission electron microscopy (TEM) analyses did not reveal noticeable structural differences

201   between both genotypes (Fig. S3). On the functional side, we tested the neutrophils ability to kill

202   microorganisms, especially fungi, as CARD9 plays a crucial role in host defense against fungal

203   infection in both humans and mice[25,20]. Indeed, *C. albicans* killing capacities are strongly affected by

204   *Card9* deletion in neutrophils (Fig. 4). An endpoint-dilution survival assay in 96-well plates revealed

205   that twice as many *C. albicans* cfu (colony forming unit) do survive after 24h co-incubation with $Card9^{-}$

206    $^{/-}$ or $Card9^{Mrp8cre}$ neutrophils compared to Card9WT or $Card9^{Mrp8wt}$ controls, respectively (Fig. 4A-B). A

207   killing assay using the cfu counting method on agar plates confirmed that $Card9^{Mrp8cre}$ neutrophils have

208   impaired abilities to kill *C. albicans* compared to $Card9^{Mrp8wt}$ (Fig. 4C). *Card9* deletion in neutrophils did

209   not impact phagocytosis *per se*, as shown by flow cytometry experiments using fluorescein-

210   isothiocyanate (FITC)-conjugated zymosan (from *Saccharomyces cerevisiae* cell wall), or cultures of

211   live *C. albicans*-GFP or *E. coli*-GFP (Fig. S4A-B). Moreover, we did not observe a difference in the

212   levels of Reactive Oxygen Species (ROS) production over time between neutrophils of the two

213   genotypes in response to phorbol myristate acetate (PMA), a PKC-dependent neutrophil activator, or

214   zymosan, a fungal stimulus (Fig. S4C-E). Even though *Card9* is involved in autophagy[30], this cellular

215   process did not seem to be affected by *Card9* deletion in neutrophils *in vitro*, as shown by the

216   normality of p62 and LC3BII/I ratio on western-blots (Fig. S4F).

217   We thus followed the track of fungal killing to investigate whether the absence of *Card9*

218   expression in neutrophils drives a general impairment of the immune system to control infection.

219   During a DSS-induced colitis model, we detected a slight but non-significant increase in total

220   fungi/bacteria DNA ratio at days 7 and 12 in the feces of $Card9^{Mrp8cre}$ compared to $Card9^{Mrp8wt}$ mice

221   (Fig. S4G). These data suggest a reduced ability of $Card9^{Mrp8cre}$ mice to contain fungi expansion in the

222   inflamed intestine. However, this effect might be difficult to point out due to the very low fungal

223   abundance in SPF mouse microbiota. Thus, to go further and reveal a potential phenotype, we

224   induced colitis in mice treated with a broad-spectrum antibiotic and antifongic cocktail and gavaged

225   with *C. albicans* to expand the intestinal fungal load (Fig. 4D). The increased colitis severity in

226    $Card9^{Mrp8cre}$ mice was maintained in this setting (Fig. 4E-G). *C. albicans* load was slightly increased

227   (although not statistically significant) in the caecal content (Fig. 4H-I), colon and caecal tissues (Fig.

228   4J) of $Card9^{Mrp8cre}$ mice, and the number of cfu recovered from liver, spleen and kidney were

229   significantly higher compared to $Card9^{Mrp8wt}$ mice (Fig. 4K). These results show that $Card9$ expression

230   in neutrophils is crucial to control the fungal load in the inflamed gut, the direct translocation of $C.$

231   $albicans$ from the gut to the liver, and to avoid its systemic dissemination.

232

233   **The absence of $Card9$ impacts neutrophils survival by increasing apoptosis**

234   To explore the mechanisms underlying the impaired capacity of $Card9^{Mrp8cre}$ neutrophils to kill

235   $C.\ albicans$ despite intact phagocytosis, autophagy, and ROS production, we investigated neutrophils

236   survival rates by flow cytometry using an AnnexinV-FITC assay coupled to Live/Dead staining (Fig. 5).

237   AnnexinV reveals ongoing apoptosis, whereas Live/Dead only stains permeable dead cells.

238   Interestingly, after 1h incubation at 37°C, $Card9^{Mrp8cre}$ neutrophils showed a significant increase in

239   AnnexinV-FITC MFI compared to $Card9^{Mrp8wt}$ neutrophils (Fig. 5A-B). Consistently, an increase in

240   percentages of apoptotic (Q1, AnnexinV$^+$LD$^-$) and dead (late apoptotic/necrotic) neutrophils (Q2,

241   AnnexinV$^+$LD$^+$), and a decrease in viable neutrophils (Q4, AnnexinV$^-$LD$^-$), were observed for the

242   $Card9^{Mrp8cre}$ genotype (Fig. 5C). Interestingly, the surface expression of the CD62L marker (a surface

243   protein that is lost upon cell activation) was reduced in $Card9^{Mrp8cre}$, with a lower percentage of CD62L$^+$

244   cells and a higher percentage of CD62L$^-$ cells (Fig. 5D). These results suggest an excessive basal

245   activation of $Card9^{Mrp8cre}$ compared to $Card9^{Mrp8wt}$ neutrophils. Similar results were obtained with

246   $Card9^{-/-}$ versus Card9WT neutrophils (Fig. S5A-D), confirming the impact of $Card9$ on neutrophil

247   survival.

248   To go further, we performed a proteomic analysis on $Card9^{Mrp8cre}$ versus $Card9^{Mrp8wt}$

249   neutrophils after 1h incubation at 37°C. This approach revealed that a large number of proteins related

250   to cellular metabolism pathways were differentially regulated between both genotypes. Indeed, a Gene

251   Ontology (GO) functional analysis showed the enrichment in numerous cellular metabolic processes,

252   both in unstimulated and stimulated conditions, among proteins statistically down- or up-regulated in

253   $Card9^{Mrp8cre}$ compared to $Card9^{Mrp8wt}$ neutrophils (Fig. 5E and S5E). Especially, we observed a high

254   prevalence of mitochondrial proteins among the differentially regulated candidates between the two

255   genotypes (Fig. 5F), suggesting that neutrophil mitochondrial functions are impacted by the absence

256   of $Card9$.

257

9

258 ***Card9* controls neutrophil survival by affecting mitochondrial function**

259 Subsequently, we analyzed neutrophil mitochondrial function using MitoTracker Green (reflecting

260 mitochondrial mass) and MitoTracker Red (reflecting mitochondrial membrane potential) markers in a

261 flow cytometry assay (Fig. 6A). No difference was observed in terms of MFIs, but we observed a

262 significant increase in the percentage of MitoGreen$^+$MitoRed$^-$ neutrophils (with dysfunctional or

263 metabolically inactive mitochondria) in the *Card9*^{Mrp8cre} compared to the *Card9*^{Mrp8wt} genotype (Fig. 6A).

264 Tetramethylrhodamine methyl ester (TMRM) assay evaluating the mitochondrial membrane potential

265 confirmed the increase in apoptotic, metabolically stressed cells (TMRM$^-$) among *Card9*^{Mrp8cre}

266 neutrophils (Fig. 6B). These results suggest that the survival defect of *Card9*^{Mrp8cre} neutrophils may be

267 due to an altered energetic metabolism. Real-time bioenergetic profile analysis using Seahorse

268 technology showed that *Card9*^{Mrp8cre} neutrophils have a higher basal Oxygen Consumption Rate

269 (OCR) during a cell mito stress assay (Fig. 6C), indicating a higher oxidative phosphorylation activity

270 compared to *Card9*^{Mrp8wt} neutrophils. Basal respiration and ATP production rate were both highly

271 increased in *Card9*^{Mrp8cre} neutrophils (Fig. 6D). Moreover, a Seahorse real-time ATP rate assay

272 demonstrated that *Card9*^{Mrp8cre} neutrophils have an increased mitochondrial ATP (mitoATP) production

273 rate, whereas glycolytic ATP (glycoATP) production rate is only mildly decreased, as shown by the

274 ATP rate index and the energetic map (Fig. 6E). A Seahorse glycolytic rate assay confirmed the

275 moderate decrease of the basal Extracellular Acidification Rate (ECAR) of *Card9*^{Mrp8cre} neutrophils

276 (Fig. S6A). However, metabolomics analysis on neutrophil supernatants incubated for 24h revealed a

277 decreased in lactate production, leading to a reduced lactate/glucose ratio in *Card9*^{Mrp8cre} neutrophils

278 (Fig. S6B). Similar results were obtained when we compared Card9WT and *Card9*$^{-/-}$ neutrophils in the

279 assays described above (Fig. S6C-E). Thus, *Card9* deletion in neutrophils induces an overactivation of

280 mitochondria and tends to reduce glycolytic activity, which is the major energy source of normal

281 neutrophils. Blocking glycolysis with 2DG (2-Deoxy-D-glucose) increased the apoptotic rate of

282 *Card9*^{Mrp8wt} but not of *Card9*^{Mrp8cre} neutrophils; showing that glycolysis is more essential to *Card9*^{Mrp8wt}

283 than *Card9*^{Mrp8cre} neutrophils (Fig.6F). Conversely, blocking the mitochondrial respiratory chain with

284 oligomycineA increased the apoptotic rate of *Card9*^{Mrp8cre} but not of *Card9*^{Mrp8wt} neutrophils,

285 demonstrating the crucial role of mitochondria as an energy source in *Card9*^{Mrp8cre} neutrophils (Fig.

286 6G). Thus, contrary to *Card9*^{Mrp8wt} neutrophils that mainly rely on glycolysis as a source of energy,

287 *Card9*^{Mrp8cre} neutrophils present an altered metabolism with an overactivation of mitochondria

10

288   associated with a dysfunctional state, leading to apoptosis. Intestinal inflammation is associated with a

289   high degree of oxidative stress. To evaluate the effect of oxidative stress on the phenotype of

290   *Card9*[Mrp8cre] neutrophils, they were treated for 1h with H_2O_2. The increased apoptosis and necrosis

291   rates observed in *Card9*[Mrp8cre] neutrophils were stronger in oxidative stress than in basal condition

292   (Fig. 6H). These results show that the role of CARD9 in the survival capacity of neutrophils, especially

293   in oxidative conditions, is mediated by effects on mitochondrial functions.

294

295   **DISCUSSION**

296   Altogether, this study reveals that, in the absence of CARD9, mitochondrial dysfunction in

297   neutrophils leads to their premature death through apoptosis, especially in an oxidative environment.

298   The decrease of functional neutrophils in the gut affects fungal containment and increases

299   susceptibility to intestinal inflammation. CARD9 polymorphisms are associated with IBD. Mouse

300   studies showed the contribution of CARD9 to host defense and intestinal barrier, notably through the

301   production of IL-22 and the modulation of the gut microbiota metabolic activity[25,26]. However, the role

302   of CARD9 in disease pathogenesis has not been elucidated at the cellular level. Our study reveals that

303   *Card9* deletion in neutrophils, contrarily to epithelial or CD11c^{+} cells, increases the susceptibility to

304   DSS-induced colitis. We thus focused on studying the role of CARD9 expression in neutrophil

305   functionality. Indeed, neutrophils have been studied in different models of IBD and fungal infection, but

306   their direct contribution to pathogenesis and the role of CARD9 in these mechanisms remain poorly

307   understood[31,4,5,32].

308   Human CARD9 deficiency results in impaired neutrophil fungal killing, leading to a selective

309   defect to contain invasive fungal infection[33]. In both humans and mice, CARD9 is required in microglia

310   for neutrophil recruitment and control of fungal infection in the central nervous system[34,35]. CARD9

311   signaling was also involved in neutrophil phagocytosis and NETosis (Neutrophil extracellular traps)

312   functions, enhancing mouse survival to a lethal dose of *C. albicans*[36]. Moreover, CARD9 expression in

313   neutrophils promotes autoantibody-induced arthritis and dermatitis in mice[37], and inflammation levels

314   in a mouse model of neutrophilic dermatosis[38]. In line with these studies, we found that *Card9* deletion

315   affects the capacity of neutrophils to kill fungi *in vitro* and *in vivo*, with no impact on neutrophil

316   structure, ROS production, autophagy or phagocytosis. We have not examined the role of CARD9 in

11

317 chemotaxis because, in the context of fungal infection in patients with CARD9 deficiency, neutrophil-

318 intrinsic chemotaxis was not affected[24]. In DSS-induced colitis, *Card9* deficiency in neutrophils does

319 not impact their recruitment to the colon, but reduces the number of mature neutrophils. Indeed, we

320 discovered that the absence of CARD9 increases apoptosis rates in neutrophils, and that this

321 premature death was caused by mitochondria overactivation. Indeed, the intrinsic pathway of

322 apoptosis is initiated by the permeabilization of mitochondria, which releases proapoptotic factors into

323 the cytosol[39,40]. Other CARD proteins mediate apoptotic signaling through CARD-CARD domain

324 interactions[13]. In addition to mediating inflammation, CARD9, a member of the CARD proteins family,

325 was recently shown to inhibit mitochondria-dependent apoptosis of cardiomyocytes under oxidative

326 stress[41]. Here, we show that CARD9 also mediates mitochondrial function and apoptosis in

327 neutrophils, especially in an oxidative environment. Further investigation is required to fully elucidate

328 the impact of mitochondria overactivation on neutrophil function, especially *in vivo*. The impact of

329 *Card9* on neutrophil mitochondrial function might not fully explain the increased susceptibility of

330 *Card9*[Mrp8cre] mice to DSS colitis. Moreover, other cell types are likely involved in the *Card9*^{-/-} mice

331 phenotype, explaining the impact of *Card9* deletion on microbiota metabolic activity, as we show that

332 this is not dependent on neutrophils[25,26].

333   Neutrophils contain very few mitochondria compared to other leukocytes, and depend mainly

334 on glycolysis to produce ATP, which is essential to perform their designated tasks. This allows energy

335 generation in a low-oxygen environment and keeps oxygen available for neutrophil effector

336 functions[42]. Thus, the dependence of neutrophils on glycolysis could be an adaptation to allow oxygen

337 to be used in the anti-microbial response rather than entering oxidative phosphorylation[42]. Here, we

338 show that in the absence of CARD9, mitochondria are overactivated in neutrophils, leading to their

339 premature death and the loss of their anti-microbial functions. Alternatively, excessive oxidative

340 phosphorylation could also lead to an overactivation of neutrophils by increasing ATP production,

341 especially in inflammatory environments where their activity is typically tightly controlled by the low

342 oxygen pressure. Neutrophil overactivation could damage the surrounding tissues and exacerbate

343 inflammation, explaining the increased susceptibility to intestinal colitis in the absence of *Card9*. In

344 humans, the « glycogen storage disease type Ib » induces a functional defect of neutrophils due to

345 glycolysis dysfunction and impaired energy homeostasis[43]. This disease is associated with IBD-like

346 phenotypes, highlighting the importance of neutrophil metabolism in intestinal health[44,43].

12

347   Immunometabolism is a central concept as immunity and metabolism impact each other in both ways :

348   (i) energetic metabolism impacts immune function, which is well-documented for lymphocytes and

349   macrophages[45], but not for neutrophils; and (ii) we show that a protein known for its roles in innate

350   immunity, CARD9, can also impact cell metabolism. Further investigation is required to understand

351   how CARD9 does interact with mitochondrial function in a direct or indirect manner.

352   Neutrophils are involved in various diseases, including infection, cardiovascular diseases,

353   inflammatory disorders and cancer, which makes them exciting targets for therapeutic intervention[46].

354   Despite the complex implication of neutrophils in disease, various therapeutic approaches aim to

355   enhance, inhibit or restore neutrophil function, depending on the pathology. In inflammatory diseases

356   with excessive neutrophil activity, their attenuation could be desired, even though killing functions

357   against microorganisms might still need to be preserved. Our work shows that increased apoptosis in

358   neutrophils does not alleviate intestinal inflammation, even though these cells are known to contribute

359   to disease development. Recent studies indicate substantial phenotypic and functional heterogeneity

360   of neutrophils[46]. Thus, targeting a specific subpopulation may allow the attenuation of harmful aspects

361   of neutrophils without compromising host defence. Some neutrophil-targeted therapeutic strategies

362   have reached the clinic, notably in the context of IBD with positive effects of the growth factor

363   granulocyte colony-stimulating factor G-CSF[47]. It opens promising options for numerous complex

364   pathologies.

365

Author Contributions

367   C.D and H.S. conceived and designed the study, performed data analysis, and wrote the manuscript;

368   C.D. designed and conducted all experiments, unless otherwise indicated; C.M., J.P., A.M., A.A., M.-

369   L.M., B. L., G.D.-C., M.S., C. G., M.P., Y.W., A.L. provided technical help for the *in vitro* and/or *in vivo*

370   experiments; J.S. and B.M. performed the immunofluorescence microscopy experiments; C.Pi. and

371   S.C. conducted the proteomics analyses; F.B., E.C. and A.R. performed the metobolomics analysis;

372   T.L. provided mice and C.O. performed genotyping; C.Pe., S.L. and J.E.-B. helped with ROS

373   production assays; R.J.A provided Scenith kits for tests with neutrophils; C.D., C.M., J.P., M.L.-R.,

374   P.L., N.R., J.E.-B., B. M. and H.S. discussed experiments and results.

375

Acknowledgments

Declaration of Interests

The authors declare no competing interests.

Material and Methods

Mice. *Card9*^{-/-}, *Rag2*^{-/-}x*Card9*^{-/-}, *Rag2*^{-/-}, *Card9*loxxMrp8cre, *Card9*loxxVillincre, and *Card9*loxxCD11ccre mice on C57BL/6J background were obtained from the Saint-Antoine Research Center and housed at the IERP (INRAE, Jouy-en-Josas) under specific pathogen-free conditions. Animal experiments were performed according to the institutional guidelines approved by the local ethics committee of the French authorities, the 'Comité d'Ethique en Experimentation Animale' (COMETHEA, CEEA45).

Induction of DSS colitis and colonization with *C. albicans*. Mice were administered drinking water supplemented with 2-3% (wt/vol) DSS (MP Biomedicals) for 5-7 days (depending on colitis severity of each experiment), and then water only for 5d. Animals were monitored daily for weight loss. For *C. albicans* colonization, mice were treated with 0.4mg/ml streptomycin, 300U/ml penicillin G and 0.125mg/ml fluconazole as indicated on Fig. 4.

14

403

404 **Histology.** Colon samples were fixed, embedded in paraffin and stained with hematoxylin and eosin.

405 Slides were scanned and analyzed to determine the histological score (Table S1)[25].

406

407 **Table S1. Histological grading of colitis**

Feature graded	Grade	Description
Inflammation severity	0	None
	1	Slight
	2	Moderate
	3	Severe
Inflammation extent	0	None
	1	Mucosa
	2	Mucosa and submucosa
	3	Transmural
Crypt damage	0	None
	1	Basal 1/3 damaged
	2	Basal 2/3 damaged
	3	Only surface epithelium lost
	4	Entire crypt and epithelium lost
Percent involvement	1	1-25%
	2	26-50%
	3	51-75%
	4	76-100%

For each feature, the product of the grade and the percentage involvement was established. The histological score was obtained by adding the subscores of each feature.

408

409 **Fecal DNA extraction and total bacteria and fungi quantification.** Fecal DNA was extracted as

410 previously described[26]. Luna Universal qPCR Master Mix (New England Biolabs) was used for

411 quantification of fungal ITS2 sequences and TaqMan Gene Expression Assays (Life Technologies) for

412 quantification of bacterial 16S rDNA sequences.

413

414 **Cell preparation and stimulation.** Epithelial cells were isolated from colonic tissue using a

415 DTT/EDTA buffer. Neutrophils were purified from mouse bone marrow using anti-Ly6G MicroBeads

416 UltraPure and MACS separation columns (Miltenyi Biotec). CD11c$^+$ cells were purified from mouse

417 spleen using anti-CD11c MicroBeads UltraPure and MACS separation columns (Miltenyi Biotec).

418 Purity checks and cell counts were performed using a BD Accuri C6 flow cytometer (BD Biosciences).

419 After purification, neutrophils were seeded in 96-well suspension plate (Sarstedt), rested for 30min in

420 RPMI 1640 Medium (Gibco, ThermoFisher Scientific) before addition of 2% heat-inactivated Fetal

421 Bovine Serum (FBS), 2-DG 10mM, oligomycine 1.5µM or H2O2 0.01M and incubated at 37°C as

422 indicated. Isolation of lamina propria immune cells was performed as previously described[48].

15

423

424 **Gene expression analysis using quantitative RT-PCR.** Total RNA was isolated from colon samples

425 or cell suspensions using RNeasy Mini Kit (Qiagen), and quantitative RT-PCR performed using

426 QuantiTect Reverse Transcription Kit (Qiagen) and Luna® Universal RT-PCR Kit (New England

427 Biolabs) in a StepOnePlus apparatus (Applied Biosystems) with specific mouse oligonucleotides

428 (Table S2). We used the $2-\Delta\Delta^{Ct}$ quantification method with mouse *Gapdh* as an endogenous control

429 and the WT group as a calibrator.

430

431 **Table S2 List of oligonucleotides and antibodies**

Oligonucleotides	SEQUENCE/SOURCE	IDENTIFIER
Gapdh (sense)	AAC TTT GGC ATT GTG GAA GG	
Gapdh (antisense)	ACA CAT TGG GGG TAG GAA CA	
*Card9*exon1F (sense)	CAG TGA CCC CAA CCT GGT CAT	
*Card9*exon3R (antisense)	TCT GCA GCT TCA TGA CCT CTG TC	
All fungi (sense) (ITS1, ITS2)	CTT GGT CAT TTA GAG GAA GTA A	
All fungi (antisense) (ITS1, ITS2)	GCT GCG TTC TTC ATC GAT GC	
All bacteria (sense) (16s)	CGG TGA ATA CGT TCC CGG	
All bacteria (antisense) (16s)	TAC GGC TAC CTT GTT ACG ACT T	
All bacteria (Probe) (16s)	6FAM-CTT GTA CAC ACC GCC CGT C-MGB	
Il-23 mouse (sense)	AGC GGG ACA TAT GAA TCT ACT AAG AGA	
Il-23 mouse (antisense)	GTC CTA GTA GGG AGG TGT GAA GTT G	
Lcn2 mouse	Quantitect	Mn_Lcn2_1_SG QT00113407
Cxcr2 mouse (sense)	CTC ACA AAC AGC GTC GTA GAA C	
Cxcr2 mouse (antisense)	AGG GCA TGC CAG AGC TAT AAT	
S100a8 mouse (sense)	TCA AGA CAT CGT TTG AAA GGA AAT C	
S100a8 mouse (antisense)	GGT AGA CAT CAA TGA GGT TGC TC	
Antibodies		
CARD9 (A-8)	Santa Cruz Biotechnology	Cat# sc-374569
β-ACTIN (D6A8)	Cell Signaling Technology	Cat# 8457S
APC-labeled anti-mouse TCRγδ (GL3)	eBioscience	Cat# 17-5711-82
anti-CD16/32 (93)	eBioscience	Cat# 14-0161-85
PerCP5.5-labeled anti-mouse CD45 (30-F11)	eBioscience	Cat# 45-0451-82
FITC–labeled anti-mouse CD3ε (145-2C11)	eBioscience	Cat# 11-0031-85

BV605-labeled anti-mouse CD8α (53-6.7)	BioLegend	Cat# 100744
PE-labeled anti-mouse CD4 (RM4-5)	eBioscience	Cat# 12-0042-83
AF700-labelled CD19 (6D5)	BioLegend	Cat# 115528
PE-labelled CD11c (N418)	BioLegend	Cat# 117308
APC-labelled F4/80 (BM8)	BioLegend	Cat# 123116
AF700-labelled CD11b (M1/70)	BioLegend	Cat# 101222
APCFire750-labelled CD45 (30-F11)	BioLegend	Cat# 103154
PerCP5.5-labelled Ly6G (1A8)	BioLegend	Cat# 127616
PE-labelled CD11b (M1/70)	eBioscence	Cat# 12-0112-82
BV421-labelled CD62L (MEL-14)	BioLegend	Cat# 104424

432

433 **Immunoblot Analysis**. Mouse tissue or cell suspensions were lysed using Laemmli buffer, loaded on

434 a SDS-PAGE and analyzed with antibodies against CARD9 (A-8:sc-374569, Santa Cruz

435 Biotechnology), or β-ACTIN (D6A8, CST).

436

437 **Flow cytometry, cell sorting and functional assays.** Flow cytometry was carried out by using LSR

438 Fortessa X-20 (BD) and cell sorting FACS Aria machines (BD). For apoptosis assay, $4x10^5$ neutrophils

439 were stained with AnnexinV-FITC in Binding Buffer (Miltenyi Biotec). For mitochondria analyses,

440 MitoTracker™ Green and MitoTracker™ Red FM were added to neutrophils in MACS buffer for 15min

441 at RT (ThermoFisher Scientific). Alternatively, neutrophils were incubated with TMRM in RPMI for

442 20min at 37°C (Abcam). For phagocytosis assay, 10^5 neutrophils stimulated with zymosan-FITC

443 (50μg/ml, Fluorescein zymosanA BioParticles conjugates, FisherScientific), *C. albicans*-GFP (MOI1:1)

444 or *Escherichia coli*-GFP (MOI1:10) for 45min. Cells were stained with surface antibodies in MACS

445 buffer (Table S2).

446

447 **Endpoint dilution survival assay**. Isolated mouse neutrophils were seeded at 10^5 cells/well in 96-

448 well plates in RPMI+2% FBS and infected with *C. albicans* (serial fourfold dilutions of an OD=1

449 solution were added by raws (row1, MOI20:1; row2, MOI5:1…). After 24h at 37°C, colonies were

450 visualized with a Nikon TMS inverted microscope and counted at the lowest dilutions (row7-8).

451

452 **Killing assay.** Purified neutrophils were seeded in 96-well plate at 10^6 cells/well and stimulated with

453 PBS, *C. albicans* (MOI1) or *E. coli* (MOI10) for 90min at 37°C. Cells were washed and lysed with

454 200μl TritonX100 0.025%. Serial dilutions were plated on YEPD or LB plates.

455

456 **Oxydative burst**. Experiments were performed on a TriStar LB942 Reader using 10^5 neutrophils in

457 200µL HBSS (ThermoFisher Scientific) and luminol 80µM (Sigma) and stimulated with phorbol 12-

458 myristate 13-acetate (PMA; 0.1µg/mL; Sigma) or opsonized zymosan (20mg/mL zymosan A from

459 *Saccharomyces cerevisiae*; Sigma). The indexed maximal relative luminescence (in relative light units

460 [RLU]) was calculated as follow: indexed RLU max=([hemochromatosis patient maximal RLU]/[healthy

461 donor maximal RLU])×100. Alternatively, superoxyde dismutase (5Units/mL) and catalase A

462 (10Units/mL) were added to differentiate total and intracellular ROS production. Absorbance was

463 measured at 550nm for 30min.

464

465 **Real time bioenergetic profile analysis.** Mito Stress Test, Glycolytic Rate Assay and Real-time ATP

466 assay were performed on a XF96 Extracellular Flux Analyzer (Seahorse Biosciences). Mouse

467 neutrophils were seeded at $2x10^5$ cells/well in RPMI+2%FBS in 0.01% poly-L-lysine pre-coated plate.

468 After 2h rest, cells were washed in Seahorse RPMI medium and incubated for 1h at 37°C without

469 CO2. In the analyzer, oligomycin 1.5µM, FCCP 1µM, Rotenone+AntimycinA 0.5µM and 2DG 50µM

470 were injected at the indicated times. Protein standardization was performed after each experiment,

471 with no noticeable differences in protein concentration and cell phenotype.

472

473 **Electron microscopy**. Purified neutrophils were stimulated with *C. albicans* (MOI 2) or *E. coli* (MOI

474 10) for 1h at 37°C, washed in PBS and fixed. Samples preparation and SEM/TEM analyses were

475 performed at the Microscopy and Imaging Platform MIMA2 (Université Paris-Saclay, INRAE,

476 AgroParisTech, Jouy-en-Josas, France, https://doi.org/10.15454/1.5572348210007727E12).

477

478 **Proteomics.** 5µg protein extracts were submitted to in-gel digestion. Desalting was performed as

479 described before[49]. Peptides were analyzed on a nanoElute-timsTOF ProLC-MS/MS system

480 (Bruker)[50]. Raw files were analyzed using MaxQuant v1.6.10.43: database UP000000589_10090

481 (21994 entries, 17-Jun-2020). Data filtering, imputation and statistical analysis were performed with

482 ProStar Zero 1.20.0[50]. Proteins with FDR<5% (Pounds method) were significant with a fold change

483 >1.2.

484

18

485   **Nuclear Magnetic Resonance.** 200μl culture media were analyzed by 1D 1H-NMR. All NMR spectra

486   were recorded on a Bruker AvanceIII 800MHz spectrometer equipped with a QPCI 5mm cryogenic

487   probe head. Spectra were acquired and processed using the Bruker Topspin 4.0 software.

488   Quantification of glucose and lactate was performed using addition of 25% TSPd4 in D2O as internal

489   standard.

490

491   **Statistical analysis.** Statistical analysis was performed using GraphPad Prism 7 software (see figure

492   legends).

493

494   **References**

495   1.   Plichta DR, Graham DB, Subramanian S, et al. Therapeutic Opportunities in Inflammatory Bowel
496   Disease: Mechanistic Dissection of Host-Microbiome Relationships. Cell 2019;178:1041–1056.

497   2.   Graham DB, Xavier RJ. Pathway paradigms revealed from the genetics of inflammatory bowel
498   disease. Nature 2020;578:527–539.

499   3.   Dave M, Papadakis KA, Faubion WA. Immunology of Inflammatory Bowel Disease and
500   Molecular Targets for Biologics. Gastroenterology Clinics of North America 2014;43:405–424.

501   4.   Wéra O, Lancellotti P, Oury C. The Dual Role of Neutrophils in Inflammatory Bowel Diseases.
502   JCM 2016;5:118.

503   5.   Zhou GX, Liu ZJ. Potential roles of neutrophils in regulating intestinal mucosal inflammation of
504   inflammatory bowel disease: Role of neutrophils in IBD. Journal of Digestive Diseases
505   2017;18:495–503.

506   6.   Caër C, Wick MJ. Human Intestinal Mononuclear Phagocytes in Health and Inflammatory Bowel
507   Disease. Front Immunol 2020;11:410.

508   7.   Kolaczkowska E, Kubes P. Neutrophil recruitment and function in health and inflammation. Nat
509   Rev Immunol 2013;13:159–175.

510   8.   Segal AW. HOW NEUTROPHILS KILL MICROBES. Annu Rev Immunol 2005;23:197–223.

511   9.   Mulholland MW, Delaney JP, Foker JE, et al. Gastrointestinal Complications of Congenital
512   Immunodeficiency States: Annals of Surgery 1983;198:673–680.

513   10.   Segal AW. The NADPH oxidase and chronic granulomatous disease. Molecular Medicine Today
514   1996;2:129–135.

515   11.   Annabi B, Mansfield BC, Hiraiwa H, et al. The Gene for Glycogen-Storage Disease Type 1b Maps
516   to Chromosome 11q23. The American Journal of Human Genetics 1998;62:400–405.

517   12.   Uzel G, Tng E, Rosenzweig SD, et al. Reversion mutations in patients with leukocyte adhesion
518   deficiency type-1 (LAD-1). Blood 2008;111:209–218.

519   13.   Bertin J, Guo Y, Wang L, et al. CARD9 Is a Novel Caspase Recruitment Domain-containing
520   Protein That Interacts With BCL10/CLAP and Activates NF-κB. Journal of Biological Chemistry
521   2000;275:41082–41086.

522   14.   Hsu Y-MS, Zhang Y, You Y, et al. The adaptor protein CARD9 is required for innate immune
523   responses to intracellular pathogens. Nat Immunol 2007;8:198–205.

524   15.   Zhernakova A, Festen EM, Franke L, et al. Genetic Analysis of Innate Immunity in Crohn's
525   Disease and Ulcerative Colitis Identifies Two Susceptibility Loci Harboring CARD9 and IL18RAP.
526   The American Journal of Human Genetics 2008;82:1202–1210.

527   16.   Franke A, McGovern DPB, Barrett JC, et al. Genome-wide meta-analysis increases to 71 the
528   number of confirmed Crohn's disease susceptibility loci. Nat Genet 2010;42:1118–1125.

529   17.   Roth S, Ruland J. Caspase recruitment domain-containing protein 9 signaling in innate immunity
530   and inflammation. Trends in Immunology 2013;34:243–250.

531   18.   McGovern DPB, Gardet A, Törkvist L, et al. Genome-wide association identifies multiple
532   ulcerative colitis susceptibility loci. Nat Genet 2010;42:332–337.

533   19.   Strasser D, Neumann K, Bergmann H, et al. Syk Kinase-Coupled C-type Lectin Receptors Engage
534   Protein Kinase C-δ to Elicit Card9 Adaptor-Mediated Innate Immunity. Immunity 2012;36:32–
535   42.

536   20.   Lanternier F, Mahdaviani SA, Barbati E, et al. Inherited CARD9 deficiency in otherwise healthy
537   children and adults with Candida species–induced meningoencephalitis, colitis, or both. Journal
538   of Allergy and Clinical Immunology 2015;135:1558-1568.e2.

539   21.   Cao Z, Conway KL, Heath RJ, et al. Ubiquitin Ligase TRIM62 Regulates CARD9-Mediated Anti-
540   fungal Immunity and Intestinal Inflammation. Immunity 2015;43:715–726.

541   22.   LeibundGut-Landmann S, Groß O, Robinson MJ, et al. Syk- and CARD9-dependent coupling of
542   innate immunity to the induction of T helper cells that produce interleukin 17. Nat Immunol
543   2007;8:630–638.

544   23.   Glocker E-O, Hennigs A, Nabavi M, et al. A Homozygous *CARD9* Mutation in a Family with
545   Susceptibility to Fungal Infections. N Engl J Med 2009;361:1727–1735.

546   24.   Rieber N, Gazendam RP, Freeman AF, et al. Extrapulmonary Aspergillus infection in patients
547   with CARD9 deficiency. JCI Insight 2016;1. Available at:
548   https://insight.jci.org/articles/view/89890 [Accessed June 15, 2021].

549   25.   Sokol H, Conway KL, Zhang M, et al. Card9 Mediates Intestinal Epithelial Cell Restitution, T-
550   Helper 17 Responses, and Control of Bacterial Infection in Mice. Gastroenterology
551   2013;145:591-601.e3.

552   26.   Lamas B, Richard ML, Leducq V, et al. CARD9 impacts colitis by altering gut microbiota
553   metabolism of tryptophan into aryl hydrocarbon receptor ligands. Nat Med 2016;22:598–605.

554   27.   Hartjes L, Ruland J. CARD9 Signaling in Intestinal Immune Homeostasis and Oncogenesis. Front
555   Immunol 2019;10:419.

556   28.   Hara H, Ishihara C, Takeuchi A, et al. The adaptor protein CARD9 is essential for the activation
557   of myeloid cells through ITAM-associated and Toll-like receptors. Nat Immunol 2007;8:619–
558   629.

559   29.   Bergmann H, Roth S, Pechloff K, et al. Card9-dependent IL-1β regulates IL-22 production from
560   group 3 innate lymphoid cells and promotes colitis-associated cancer. Eur J Immunol
561   2017;47:1342–1353.

562   30.   Yang C-S, Rodgers M, Min C-K, et al. The Autophagy Regulator Rubicon Is a Feedback Inhibitor
563   of CARD9-Mediated Host Innate Immunity. Cell Host & Microbe 2012;11:277–289.

564   31.   Gazendam RP, Geer A van de, Roos D, et al. How neutrophils kill fungi. Immunol Rev
565   2016;273:299–311.

566   32.   Desai JV, Lionakis MS. The Role of Neutrophils in Host Defense Against Invasive Fungal
567   Infections. Curr Clin Micro Rpt 2018;5:181–189.

568   33.   Drewniak A, Gazendam RP, Tool ATJ, et al. Invasive fungal infection and impaired neutrophil
569   killing in human CARD9 deficiency. Blood 2013;121:2385–2392.

570   34.   Drummond RA, Collar AL, Swamydas M, et al. CARD9-Dependent Neutrophil Recruitment
571   Protects against Fungal Invasion of the Central Nervous System May RC, ed. PLoS Pathog
572   2015;11:e1005293.

573   35.   Drummond RA, Swamydas M, Oikonomou V, et al. CARD9+ microglia promote antifungal
574   immunity via IL-1β- and CXCL1-mediated neutrophil recruitment. Nat Immunol 2019;20:559–
575   570.

576   36.   Loh JT, Xu S, Huo JX, et al. Dok3–protein phosphatase 1 interaction attenuates Card9 signaling
577   and neutrophil-dependent antifungal immunity. Journal of Clinical Investigation
578   2019;129:2717–2729.

579   37.   Németh T, Futosi K, Sitaru C, et al. Neutrophil-specific deletion of the CARD9 gene expression
580   regulator suppresses autoantibody-induced inflammation in vivo. Nat Commun 2016;7:11004.

581   38.   Tartey S, Gurung P, Samir P, et al. Cutting Edge: Dysregulated CARD9 Signaling in Neutrophils
582   Drives Inflammation in a Mouse Model of Neutrophilic Dermatoses. JI 2018;201:1639–1644.

583   39.   Kobayashi SD, Malachowa N, DeLeo FR. Influence of Microbes on Neutrophil Life and Death.
584   Front Cell Infect Microbiol 2017;7:159.

585   40.   McCracken JM, Allen L-AH. Regulation of Human Neutrophil Apoptosis and Lifespan in Health
586   and Disease. J□Cell Death 2014;7:JCD.S11038.

587   41.   Li Y, Liang P, Jiang B, et al. CARD9 inhibits mitochondria-dependent apoptosis of
588   cardiomyocytes under oxidative stress via interacting with Apaf-1. Free Radical Biology and
589   Medicine 2019;141:172–181.

590   42.   Burn GL, Foti A, Marsman G, et al. The Neutrophil. Immunity 2021;54:1377–1391.

591   43.   Jun HS, Weinstein DA, Lee YM, et al. Molecular mechanisms of neutrophil dysfunction in
592   glycogen storage disease type Ib. Blood 2014;123:2843–2853.

593   44.   Yamaguchi T, Ihara K, Matsumoto T, et al. Inflammatory Bowel Disease-Like Colitis in Glycogen
594   Storage Disease Type 1b: Inflammatory Bowel Diseases 2001;7:128–132.

595   45.   Makowski L, Chaib M, Rathmell JC. Immunometabolism: From basic mechanisms to translation.
596   Immunol Rev 2020;295:5–14.

597   46.   Németh T, Sperandio M, Mócsai A. Neutrophils as emerging therapeutic targets. Nat Rev Drug
598   Discov 2020;19:253–275.

599   47.   Guidi L. Treatment of Crohn’s disease with colony-stimulating factors: An overview.
600   TCRM 2008;Volume 4:927–934.

601   48.   Dupraz L, Magniez A, Rolhion N, et al. Gut microbiota-derived short-chain fatty acids regulate
602   IL-17 production by mouse and human intestinal γδ T cells. Cell Reports 2021;36:109332.

603   49.   Hamada S, Pionneau C, Parizot C, et al. In-depth proteomic analysis of *Plasmodium berghei*
604   sporozoites using trapped ion mobility spectrometry with parallel accumulation-serial
605   fragmentation. Proteomics 2021;21:2000305.

606   50.   Pereira M, Richetta C, Sarango G, et al. *The Autophagy Receptor TAX1BP1 (T6BP) is a novel*
607   *player in antigen presentation by MHC-II molecules*. Immunology; 2021. Available at:
608   http://biorxiv.org/lookup/doi/10.1101/2021.04.21.440798 [Accessed December 17, 2021].

609

610   **Main figure titles and legends**

611   **Figure 1. Lymphocytes have no intrinsic role in the *Card9*^{-/-} phenotype in colitis models.** (A)

612   Weight and (B) Disease Activity Index (DAI) score of DSS-exposed *Rag2*^{-/-} or *Rag2*^{-/-} x *Card9*^{-/-} mice.

613   (C) Colon length and (D) histological score of colon sections at day 7. Data points represent individual

614   mice. One representative experiment out of three. (E) Representative H&E-stained images of mid

615   colon cross-sections from DSS-exposed *Rag2*^{-/-} (left) and *Rag2*^{-/-} x *Card9*^{-/-} (right) mice at day 7. Scale

616   bars, 500 μm. (F) Weight of mice receiving naive T cells for adoptive transfer of colitis experiment.

617   *Rag2*^{-/-} received either WT or *Card9*^{-/-} lymphocytes. *Rag2*^{-/-} x *Card9*^{-/-} mice received WT lymphocytes.

618   Data are mean ± SEM of two independent experiments. *P<0.05, **P<0.01, ***P<0.001, ****P<0.0001

619   as determined by two-way analysis of variance (ANOVA) with Sidak's post-test (A, B, F) and Mann-

620   Whitney test (C, D). LT, lymphocytes T.

621   **Figure 2. *Card9* expression in neutrophils, but not in epithelial or CD11c⁺ cells, protects against**

622   **colitis.** (A) Weight and DAI score of DSS-exposed *Card9*^{Villinwt} or *Card9*^{Villincre} mice. (B) Weight and

623   DAI score of DSS-exposed *Card9*^{cd11cwt} or *Card9*^{cd11ccre} mice. (C) Weight and DAI score of DSS-

624   exposed *Card9*^{Mrp8wt} or *Card9*^{Mrp8cre} mice. (D) Colon length, (E) histological score of colon sections and

625   (F) representative H&E-stained images of mid colon cross-sections from DSS-exposed *Card9*^{Mrp8wt}

626   (left) and *Card9*^{Mrp8cre} (right) mice at day 12. Scale bars, 500 μm. (G) Myeloperoxidase (MPO)

627   concentration in total colon tissue at day 12. (H) Lipocalin (*Lcn2*) expression by qRT-PCR in total

628   colon tissue at day 12, normalized to *Gapdh*. Data points represent individual mice. Data are mean ±

629   SEM of three independent experiments. *P<0.05, **P<0.01, ***P<0.001, ****P<0.0001 as determined

630   by two-way ANOVA with Sidak's post-test (A-C) and Mann-Whitney test (D-H).

631   **Figure 3. *Card9* deletion affects the number of neutrophils in the inflamed colon.** (A) Relative

632   expression of *Lcn2*, *Cxcr2* and *S1008a* in distal colon tissue of C57BL/6 WT mice during a DSS colitis

633   model relative to *Gapdh*. (B) Representative H&E-stained images of mid colon cross-sections from

634   DSS-exposed WT mice at day 0, 4, 7, 9, 12 and 16 after DSS exposure. Scale bars, 50 μm. (C) *Lcn2*,

635   *Cxcr2* and *S100A8* expression in total colon tissue from *Card9*^{Mrp8wt} and *Card9*^{Mrp8cre} mice at day 9 of

636   DSS colitis by qRT-PCR analyses, normalized to *Gapdh*. (D) Representative flow cytometry plots of

637   Ly6G⁺CD11b⁺ cells (neutrophils) in the colon lamina propria (LP) of DSS-exposed *Card9*^{Mrp8wt} and

638   *Card9*^{Mrp8cre} mice. (E) Percentage and count of Ly6G⁺CD11b⁺ cells in the LP of DSS-exposed

639   *Card9*^{Mrp8wt} and *Card9*^{Mrp8cre} mice. (F) Ly6G and (G) CD11b expression (MFI for Mean Fluorescence

640   Intensity) of Ly6G⁺CD11b⁺ neutrophils from *Card9*^{Mrp8wt} and *Card9*^{Mrp8cre} mice. Data points represent

641   individual mice. Data are mean ± SEM of two independent experiments. *P<0.05, **P<0.01,

642   ***P<0.001 as determined by Mann-Whitney tests.

643   **Figure 4. *C. albicans* killing capacity is impacted by *Card9* deletion in neutrophils.** (A)

644   Representative images of *C. albicans* cfu number at the endpoint dilution after infection of *Card9*WT,

645   *Card9*^{-/-}, *Card9*^{Mrp8wt} or *Card9*^{Mrp8cre} neutrophils for 24h, using a microscope (top) or directly showing *C.*

646   *albicans* cfu in the 96-well plate, with a photography from above (middle picture) or a scan from below

647   the plate (bottom picture). (B) *C. albicans* cfu after infection of neutrophils for 24h. Cfu counting was

648   performed in 96 well plates using a microscope. Data points represent individual mice. Data are mean

649   ± SEM of three independent experiments. (C) *C. albicans* cfu number after infection of *Card9*^{Mrp8wt} or

650   *Card9*^{Mrp8cre} neutrophils for 3 or 24h. Cfu counting was performed after plating on YEPD agar plates.

651   Data are mean ± SEM of two independent experiments. (D) Experimental design of antibiotic

652   treatments and *C. albicans* inoculation in mice treated with 3% DSS. (E) Weight, (F) DAI and (G) colon

653   length of DSS-exposed *Card9*^{Mrp8wt} and *Card9*^{Mrp8cre} mice after colonization with *C. albicans*. (H-K)

654   Fungal burden in the feces (H), caecal content (I), caecal and colon tissue (J) and liver, spleen and

655   kidney (K) of DSS-exposed *Card9*^{Mrp8wt} and *Card9*^{Mrp8cre} mice after colonization with *C. albicans*. Data

656   are mean ± SEM of two independent experiments. *P<0.05, **P<0.01, ***P<0.001, ****P<0.0001 as

657   determined by one-way ANOVA with Tukey's post-test (A), two-way ANOVA with Sidak's post-test (E,

658   F) and Mann-Whitney test (C, G, I-K). Genta, gentamycin.

659   **Figure 5. The absence of *Card9* impacts neutrophils survival by increasing apoptosis.** (A)

660   Representative flow cytometry plots of Ly6G⁺CD11b⁺ neutrophils purified from bone marrow of

661   *Card9*^{Mrp8wt} (left) and *Card9*^{Mrp8cre} (right) mice, co-stained with AnnexinV and a Live/Dead marker. (B)

662   AnnexinV MFI of Ly6G⁺CD11b⁺ neutrophils from *Card9*^{Mrp8wt} and *Card9*^{Mrp8cre} mice, incubated for 1h at

663   37°C. (C) Percentage of apoptotic neutrophils (Q1: AnnexinV⁺LD⁻ cells), dead (late apoptotic/necrotic)

664   neutrophils (Q2: AnnexinV⁺LD⁺ cells) and viable neutrophils (Q4: AnnexinV⁻LD⁻ cells) amongst the

665   Ly6G⁺CD11b⁺ population. (D) Percentage of CD62L⁺ and CD62L⁻ neutrophils amongst the

666   Ly6G⁺CD11b⁺ population. Data represent one out of two independent experiments. (E) Histogram

667   representing Gene Ontology biological processes significantly enriched amongst proteins down- (blue)

24

668   or up-regulated (red) in *Card9*[Mrp8cre] compared to *Card9*[Mrp8wt] neutrophils in the unstimulated condition.

669   (F) Morpheus heat-map representing mitochondria-related proteins significantly down- or up-regulated

670   in *Card9*[Mrp8cre] compared to *Card9*[Mrp8wt] neutrophils in the unstimulated condition. E and F obtained

671   from proteomics data analysis. *P<0.05, **P<0.01, ***P<0.001, ****P<0.0001 as determined by Mann-

672   Whitney test (B) and two-way ANOVA with Sidak's post-test (C-D).

673   **Figure 6. *Card9* controls neutrophil energetic metabolism by affecting mitochondrial function.**

674   (A) Representative flow cytometry plots and precentages of MitoGreen^{+}MitoRed^{-} cells (corresponding

675   to cells with dysfunctional mitochondria) amongst Ly6G^{+}CD11b^{+} neutrophils. Neutrophils were purified

676   from the bone marrow of *Card9*[Mrp8wt] or *Card9*[Mrp8cre] mice, and incubated for 1h at 37°C. (B)

677   Representative flow cytometry plots and percentages of TMRM^{-} cells (corresponding to cells with

678   dysfunctional mitochondria/apoptotic or metabolically inactive cells) amongst Ly6G^{+}CD11b^{+}

679   neutrophils. (C) Oxygen Consumption Rate (OCR) of *Card9*[Mrp8wt] and *Card9*[Mrp8cre] neutrophils

680   measured during a Seahorse Cell Mito Stress assay. (D) Basal respiration (late rate measurement

681   before oligomycin injection (t3) - non-mitochondrial respiration rate (t12)) and ATP production rate

682   (late rate measurement before oligomycin (ATP synthase blocker) injection (t3) – minimum rate

683   measurement after oligomycin injection (t6) obtained from the Seahorse Cell Mito Stress assay. (E)

684   ATP rate index and energetic map of *Card9*[Mrp8wt] and *Card9*[Mrp8cre] neutrophils obtained from the

685   Seahorse Real-time ATP rate assay. (F) Percentage of apoptotic cells amongst the Ly6G^{+}CD11b^{+}

686   neutrophil population of *Card9*[Mrp8wt] and *Card9*[Mrp8cre] genotypes after treatment with 2-DG 10 mM or

687   (G) oligomycin 1.5 µM for 1h. (H) Percentage of apoptotic and necrotic cells amongst the

688   Ly6G^{+}CD11b^{+} neutrophil population of *Card9*[Mrp8wt] and *Card9*[Mrp8cre] genotypes after addition of H2O2

689   0.01 mM for 1h to increase oxydative stress. Data are mean ± SEM of at least two independent

690   experiments. *P<0.05, **P<0.01, ***P<0.001, ****P<0.0001 as determined by Mann-Whitney test (A,

691   B, D, E, F) or two-way ANOVA with Sidak's post-test (G, H). Norm. Unit, normalized unit; FCCP,

692   Carbonyl cyanide 4-(trifluoromethoxy)phenylhydrazone; Rot/AA, Rotenone/AntimycinA; 2DG, 2 deoxy-

693   glucose; OligoA, oligomycinA.

694

695   **Supplemental Figure and Table**

696   **Figure S1. *Card9* is mainly expressed by myeloid cells.** (A) *Card9* expression in different organs of

697   *Card9*WT and *Card9*^{-/-} mice by quantitative RT-PCR analyses, normalized to *Gapdh*. (B) CARD9 and

698   β-ACTIN expression in different organs of *Card9*WT and *Card9*^{-/-} mice by Western Blot analyses. (C)

699   *Card9* expression in different sorted cell populations from the spleen and bone marrow of *Card9*WT

700   and *Card9*^{-/-} mice by quantitative RT-PCR analyses, normalized to *Gapdh.*

701   **Figure S2. Validation of conditional knockout mice strains.** (A) *Card9* expression in colonic

702   epithelial cells and tissue from *Card9*[Villinwt] and *Card9*[Villincre] mice (up right panel), CD11c^{+} purified cells

703   and CD11c^{-} fraction from the spleen of *Card9*[Cd11cwt] and *Card9*[Cd11ccre] mice (up left panel) and Ly6G^{+}

704   purified neutrophils and Ly6G^{-} fraction from the bone marrow of *Card9*WT, *Card9*^{-/-}, *Card9*[Mrp8wt] and

705   *Card9*[Mrp8cre] mice (lower panels) by qRT-PCR analyses, normalized to *Gapdh*. (B) CARD9 and β-

706   ACTIN expression in Ly6G^{+} purified neutrophils and Ly6G^{-} fraction from the bone marrow of *Card9*WT,

707   *Card9*^{-/-}, *Card9*[Mrp8wt] and *Card9*[Mrp8cre] mice by Western blot. (C) Flow cytometry plots representing total

708   cell populations of the bone marrow of a C57BL/6 mouse (left panel), and Ly6G^{+}CD11b^{+} neutrophils

709   purified from the bone marrow using Ly6G ultrapure magnetic beads and MACS column (right panel).

710   (D) Colon length of DSS-exposed *Card9*[Villinwt], *Card9*[Villincre], *Card9*[Cd11cwt] and *Card9*[Cd11ccre] mice. (E)

711   AhR activity of feces from *Card9*[Mrp8wt] and *Card9*[Mrp8cre] mice at steady-state, using HepG2 reporting

712   cells. (F) Weight and DAI score of DSS-exposed *Card9*[Mrp8wt] or *Card9*[Mrp8cre] mice for 9 days.

713   **Figure S3. Imaging of *Card9*-deleted neutrophils.** (A) Immunofluorescence staining of *Card9*WT,

714   *Card9*^{-/-}, *Card9*[Mrp8wt] and *Card9*[Mrp8cre] neutrophils unstimulated or stimulated with zymosan for 1 or 3h.

715   Blue for DNA, red for β-ACTIN. Scale bars, 5 μm. (B) Scanning electron microscopy (SEM, left) or

716   Transmission electron microscopy (TEM, right) of *Card9*[Mrp8wt] and *Card9*[Mrp8cre] neutrophils

717   unstimulated or stimulated with *C. albicans* or *E. coli* for 1h. White arrows point *C. albicans* or *E. coli*

718   phagocytosed by neutrophils. Scale bars, 1 or 1.5 μm.

719   **Figure S4. *C. albicans* killing capacity is impacted by *Card9* deletion in neutrophils, but not**

720   **phagocytosis capacity, ROS production or autophagy.** (A) Representative flow cytometry plots

721   showing percentages of Ly6G^{+}FITC[+] and Ly6G^{+}GFP[+] *Card9*WT or *Card9*^{-/-} neutrophils stimulated by

722   zymosan-FITC (50μg/ml, Fluorescein zymosan A BioParticles conjugates), *C. albicans*-GFP (MOI 1:1)

723   or *E. coli*-GFP (MOI 1:10) for 45 min. (B) Graph representing phagocytosis rates obtained by flow

724 cytometry analysis. (C-D) Oxydative burst kinetics of *Card9*WT, *Card9*^{-/-}, *Card9*[Mrp8wt] and *Card9*[Mrp8cre]

725 neutrophils as measured by luminol-amplified chemiluminescence of *Card9*WT and *Card9*^{-/-} (left

726 panel) and *Card9*[Mrp8wt] and *Card9*[Mrp8cre] (right panel) neutrophils after stimulation with (C) PMA

727 (phorbol 12-myristate 13-acetate; 0.1 μg/mL; Sigma) or (D) opsonized zymosan (20 mg/mL, zymosan

728 A from *Saccharomyces cerevisiae* opsonized with 10% SVF). (E) Total and Intracellular Reactive

729 Oxygen Species (ROS) produced by *Card9*WT and *Card9*^{-/-} neutrophils (left), or *Card9*[Mrp8wt] and

730 *Card9*[Mrp8cre] neutrophils (right) in unstimulated condition or after 90 min stimulation with non-opsonized

731 zymosan (0.5 mg/mL). RLU, relative light unit. (F) Western blot showing p62 (62 KDa) and

732 LC3BI/LC3BII (16 and 14 KDa) autophagy proteins in *Card9*WT, *Card9*^{-/-}, *Card9*[Mrp8wt] and *Card9*[Mrp8cre]

733 neutrophils purified from the bone marrow and incubated 1h in RPMI +2% FBS at 37°C. (G)

734 Fungi/bacteria loads in feces from *Card9*[Mrp8wt] or *Card9*[Mrp8cre] mice during DSS colitis measured by

735 qRT-PCR (ratio of 2^{-Ct}).

736 **Figure S5. The absence of *Card9* impacts neutrophils survival by increasing apoptosis.** (A)

737 Representative flow cytometry plots of Ly6G^{+}CD11b^{+} neutrophils purified from bone marrow of

738 *Card9*WT (left) and *Card9*^{-/-} (right) mice, co-stained with AnnexinV and a Live/Dead marker. (B)

739 AnnexinV MFI of Ly6G^{+}CD11b^{+} neutrophils from *Card9*WT and *Card9*^{-/-} mice, incubated for 1h at

740 37°C. (C) Percentage of apoptotic neutrophils (Q1: AnnexinV^{+}LD^{-} cells), dead (late apoptotic/necrotic)

741 neutrophils (Q2: AnnexinV^{+}LD^{+} cells) and viable neutrophils (Q4: AnnexinV^{-}LD^{-} cells) amongst the

742 Ly6G^{+}CD11b^{+} population. (D) Percentage of CD62L^{+} and CD62L^{-} neutrophils amongst the

743 Ly6G^{+}CD11b^{+} population. Data represent one out of two independent experiments. *P<0.05, **P<0.01,

744 ***P<0.001, ****P<0.0001 as determined by Mann-Whitney test (B) or two-way ANOVA with Sidak's

745 post-test (C-D).

746 **Figure S6. *Card9* controls neutrophil energetic metabolism by affecting mitochondrial function.**

747 (A) Extracellular Acidification Rate (ECAR) of *Card9*[Mrp8wt] and *Card9*[Mrp8cre] neutrophils measured

748 during a Seahorse Glycolytic rate assay in unstimulated condition (RPMI + 2% FBS). Graph

749 represents basal glycolysis (t2). (B) Lactate/glucose ratio in 24h culture supernatant of *Card9*[Mrp8wt] and

750 *Card9*[Mrp8cre] neutrophils measured by metabolomics data analyses. (C) Representative flow cytometry

751 plots and percentages of MitoGreen^{+}MitoRed^{-} cells (corresponding to cells with dysfunctional

752 mitochondria) amongst the Ly6G^{+}CD11b^{+} neutrophil population from *Card9*WT or *Card9*^{-/-} mice

753   incubated for 1h at 37°C. (D) Representative flow cytometry plots and percentages of TMRM⁻ cells

754   (corresponding to cells with dysfunctional mitochondria/apoptotic or metabolically inactive cells)

755   amongst the Ly6G$^+$CD11b$^+$ neutrophil population incubated for 3h at 37°C. (E) Oxygen Consumption

756   Rate (OCR) and Extracellular Acidification Rate (ECAR) of *Card9*WT or *Card9*$^{-/-}$ neutrophils measured

757   during a Seahorse Cell Mito Stress assay or a Seahorse Glycolytic rate assay, respectively. Data are

758   mean ± SEM of at least two independent experiments. *$P<0.05$, **$P<0.01$, ***$P<0.001$, ****$P<0.0001$

759   as determined by Mann-Whitney tests. FCCP, Carbonyl cyanide 4-(trifluoromethoxy)phenylhydrazone;

760   Rot/AA, Rotenone/AntimycinA; 2-DG, 2-deoxy-D-glucose.

761   **Table S1. Histological grading of colitis**

762   **Table S2. List of oligonucleotides and antibodies**
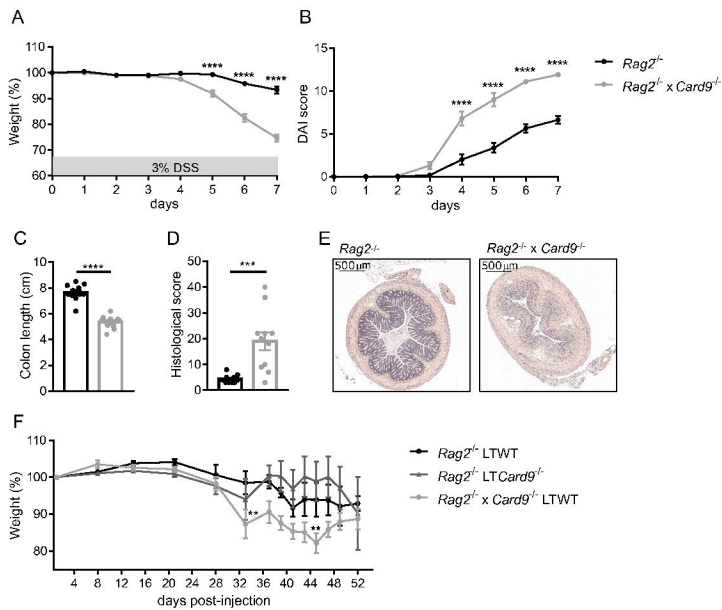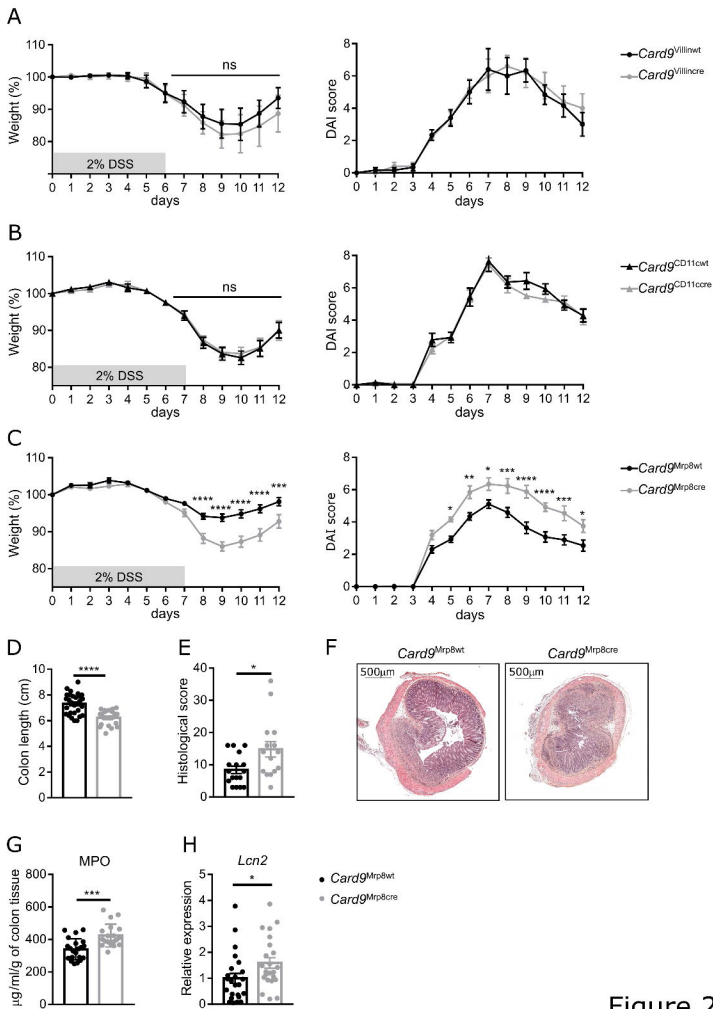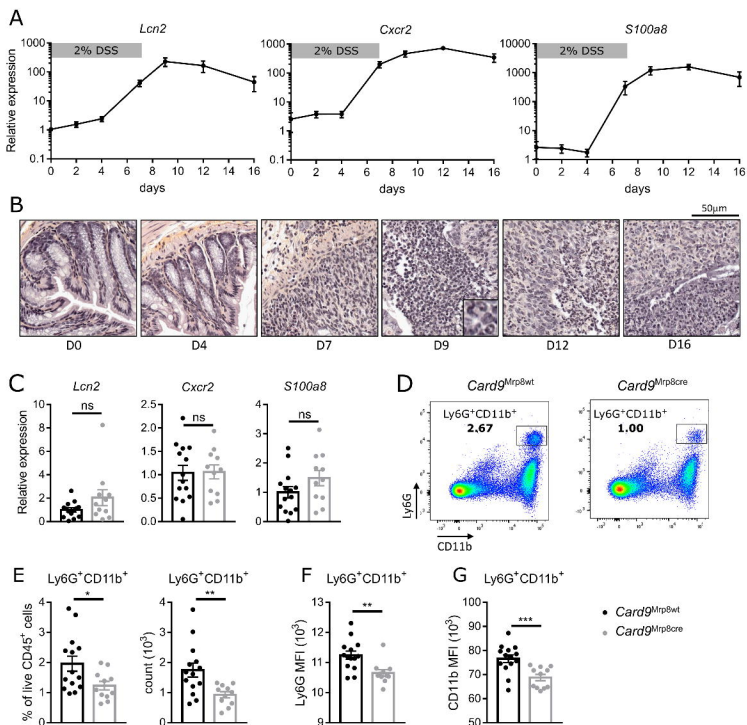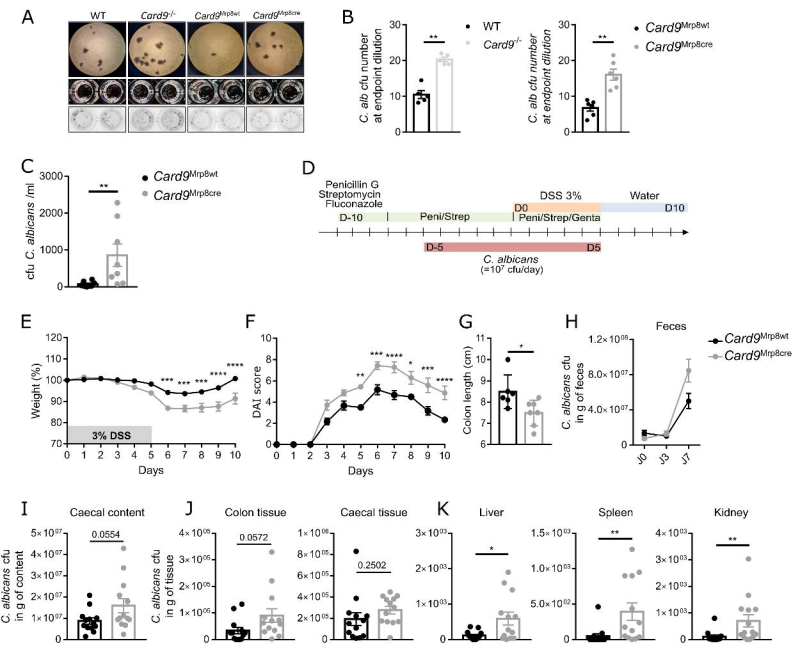
763

Figure 1

Figure 2

A

Lcn2 — 2% DSS — Relative expression vs days

Cxcr2 — 2% DSS — Relative expression vs days

S100a8 — 2% DSS — Relative expression vs days

B

D0 D4 D7 D9 D12 D16

50μm

C

Lcn2 ns

Cxcr2 ns

S100a8 ns

D

Card9^Mrp8wt   Ly6G⁺CD11b⁺ 2.67

Card9^Mrp8cre   Ly6G⁺CD11b⁺ 1.00

Ly6G vs CD11b

E

Ly6G⁺CD11b⁺ % of live CD45⁺ cells *

Ly6G⁺CD11b⁺ count (10³) **

F

Ly6G⁺CD11b⁺ Ly6G MFI (10³) **

G

Ly6G⁺CD11b⁺ CD11b MFI (10³) ***

● *Card9*^Mrp8wt
● *Card9*^Mrp8cre

Figure 3

Figure 4

Figure 5

Figure 6